Article

On the Mechanism of Hydrogen Storage in a Metal–Organic Framework Material

Jonathan L. Belof, Abraham C. Stern, Mohamed Eddaoudi, and Brian Space

J. Am. Chem. Soc., **2007**, 129 (49), 15202-15210 • DOI: 10.1021/ja0737164

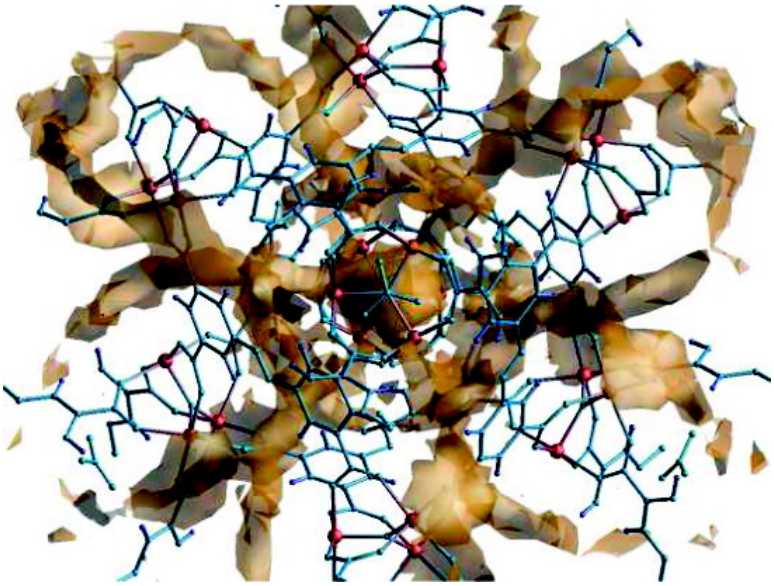

J|A|C|S
ARTICLES
Published on Web 11/14/2007

On the Mechanism of Hydrogen Storage in a Metal−Organic Framework Material

Jonathan L. Belof, Abraham C. Stern, Mohamed Eddaoudi, and Brian Space*

Contribution from the Department of Chemistry, University of South Florida, 4202 East Fowler Avenue, CHE205, Tampa, Florida 33620-5250

Received June 11, 2007; E-mail: space@cas.usf.edu

Abstract: Monte Carlo simulations were performed modeling hydrogen sorption in a recently synthesized metal−organic framework material (MOF) that exhibits large molecular hydrogen uptake capacity. The MOF is remarkable because at 78 K and 1.0 atm it sorbs hydrogen at a density near that of liquid hydrogen (at 20 K and 1.0 atm) when considering H_2 density in the pores. Unlike most other MOFs that have been investigated for hydrogen storage, it has a highly ionic framework and many relatively small channels. The simulations demonstrate that it is both of these physical characteristics that lead to relatively strong hydrogen interactions in the MOF and ultimately large hydrogen uptake. Microscopically, hydrogen interacts with the MOF via three principle attractive potential energy contributions: Van der Waals, charge-quadrupole, and induction. Previous simulations of hydrogen storage in MOFs and other materials have not focused on the role of polarization effects, but they are demonstrated here to be the dominant contribution to hydrogen physisorption. Indeed, polarization interactions in the MOF lead to two distinct populations of dipolar hydrogen that are identified from the simulations that should be experimentally discernible using, for example, Raman spectroscopy. Since polarization interactions are significantly enhanced by the presence of a charged framework with narrow pores, MOFs are excellent hydrogen storage candidates.

I. Introduction

A major obstacle in achieving a hydrogen-based fuel economy is the ability to store and transport molecular hydrogen safely at reasonable temperatures and pressures. For example, at one atmosphere, hydrogen does not liquefy until 20 K[1] because of its relatively weak intermolecular interactions, making the transport of neat hydrogen difficult. Thus, finding materials capable of storing large amounts of diatomic hydrogen is a promising avenue. The challenge is that hydrogen typically interacts weakly with its environment. However, hydrogen molecules can interact strongly with some materials, by undergoing chemisorption or dissociation, but such materials are typically inadequate for hydrogen storage because it is difficult to release the stored gas when it is needed.[2,3] On the other hand, materials that physisorb molecular hydrogen offer the promise of storing it under moderate conditions and the ability to release the hydrogen facilely. Such a material would require optimizing the attractive intermolecular interactions between the hydrogen and the condensed phase environment and, at the same time, enhancing H_2-H_2 interactions, thus leading to a favorable sorption enthalpy. The experimental[4−7] and theoretical[8−10] study of this unique problem has become an area of intense research in recent years, with a diverse range of prospective candidate materials being studied.

Metal−organic framework materials (MOFs) are a class of materials that have already shown promise for hydrogen storage.[11,12] MOFs represent a novel class of solid crystalline materials that are built with rigid organic ligands linked to metal-containing clusters (also known as secondary building units or SBUs)[13] They can be constructed to have large surface areas, are relatively light weight, and can be assembled from molecular building blocks with desired chemical functionality. Recently, a MOF was reported[11] (referred to here as *soc*-MOF) that was synthesized using a novel indium trimer building block that resulted in a nanoporous material with an ionic framework, narrow channels (around 1 nm in diameter) and nanometer scale carcerand capsules. The MOF has a rare soc topology[14] (e.g., not found in zeolites) characterized by its square-octahedral connectivity net.[15] The molecular formula, $[In_3O(C_{16}N_2O_8H_6)_{1.5}](NO_3)$, includes ionically bound nitrate anions proximal to the indium trimer. The cationic indium of the SBU possesses an

(1) Weast, R. C. *CRC Handbook of Chemistry and Physics;* CRC Press Inc.: West Palm Beach, FL, 1994.
(2) Rowsell, J. L.; Yaghi, O. M. *Angew. Chem., Int. Ed.* **2005**, *44*, 4670.
(3) Seayad, A. M.; Antonelli, D. M. *Adv. Mater.* **2004**, *16*, 765.
(4) Berube, V.; Radtke, G.; Dresselhaus, M.; Chen, G. *Int. J. Energy Res.* **2007**, *6−7*, 637.
(5) David, E. J. *Mater. Process. Technol.* **2005**, *162*, 169.
(6) Fakioglu, E.; Yurum, Y. ; Veziroglu, T. *Int. J. Hydrogen Energy* **2004**, *13*, 1371.
(7) Seayad, A.; Antonelli, D. *Adv. Mater.* **2004**, *9−10*, 765.
(8) Anderson, C.-R.; Coker, D. F.; Eckert, J.; Bug, A. L. R. *J. Chem. Phys.* **1999**, *111*, 7599.
(9) Eckert, J. *Spectrochim. Acta* **1992**, *48A*, 363.
(10) Garberoglio, G.; Skoulidas, A. I.; Johnson, J. K. *J. Phys. Chem. B* **2005**, *109*, 13094.
(11) Liu, Y.; Eubank, J. F.; Cairns, A. J.; Eckert, J.; Kravtsov, V. C.; Luebke, R.; Eddaoudi, M. *Angew. Chem., Int. Ed.* **2007**, *46*, 3278.
(12) Rosi, N. L.; Eckert, J.; Eddaoudi, M.; Vodak, D. T.; Kim, J.; O'Keeffe, M.; Yaghi, O. M. *Science* **2003**, *300*, 1127.
(13) Moulton, B.; Zaworotko, M. J. *Chem. Rev.* **2001**, *101*, 1629.
(14) O'Keeffe, M.; Yaghi, O. M. 2003; http://rcsr.anu.edu.au/.
(15) Delgado-Friedrichs, O.; O'Keeffe, M.; Yaghi, O. M. *Acta Crystallogr.* **2006**, *A62*, 350.

10.1021/ja0737164 CCC: $37.00

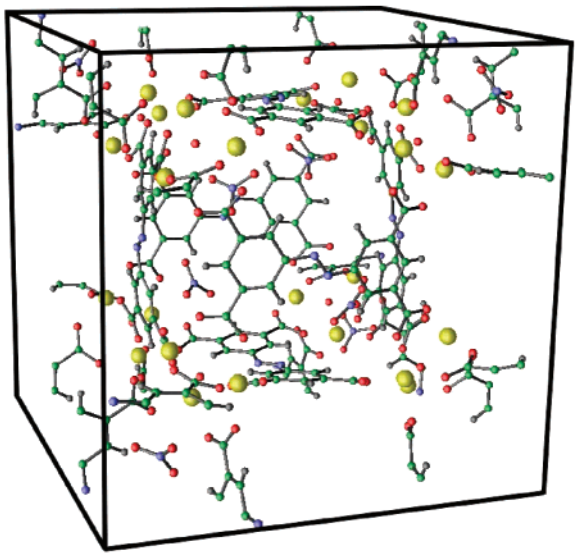

(a) *soc*-MOF empty

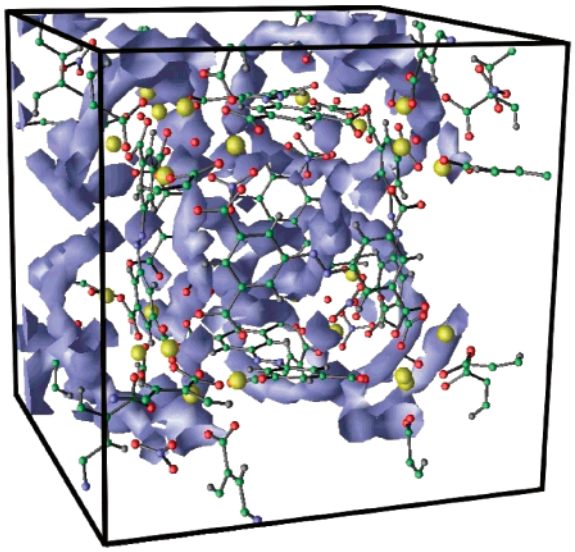

(b) *soc*-MOF populated

Figure 1. This illustration shows the *soc*-MOF both empty and populated via simulation of 113 H_2 with a polarizable model. The hydrogen density is represented by a 90% populated isosurface (generated by a custom module written for Data Explorer[17−19]) and has been rendered with a clipping plane for clarity. It should be noted that the indium (yellow) trimers are not depicted as being bonded, strictly to enhance the visibility of the structure.

open-coordination site which, along with the bound nitrate anion, contributes toward giving the framework a highly ionic character. The unit-cell has been visualized with the carcerand capsules located in the center, where each capsule contains tetrahedrally positioned nitrate anions. The MOF possesses an estimated 57% extraframework volume, a large Langmuir surface area of 1417 $m^2\ g^{-1}$, and 0.50 $cm^3\ g^{-1}$ pore volume.[11]

Figure 1 shows snapshots of *soc*-MOF alone and with a hydrogen density isosurface calculated from simulation (described later). The hydrogen is resident in the extraframework, and Figure 1 serves to visually highlight the pore topology within *soc*-MOF. Hydrogen uptake studies on *soc*-MOF show a large storage capacity with reversible sorption. For example, at 78 K and 1.0 atm, the density of H_2 in the pores is approximately 0.05 g cm^{-3}, while liquid hydrogen at its boiling point of 20 K has a density of 0.07 g cm^{-3}.[11] The experiments are conducted at liquid nitrogen temperature as a step toward finding superior hydrogen storage materials that will ultimately operate at room temperature.[16] This pore density of H_2 represents a compression factor, compared to the ideal gas under the same conditions, of approximately 100. Hydrogen sorption isotherms were measured at 78 K on *soc*-MOF and showed that the pores were filled at relatively lower pressure.[11] The MOF approached saturation at 1.0 atm, indicative of the near liquid density of the sorbed hydrogen.

Thus, to investigate the physical basis of the large hydrogen uptake, canonical Monte Carlo simulations were performed on hydrogen in *soc*-MOF (at the experimentally observed hydrogen density at 78 K and 1.0 atm). Since *soc*-MOF has a highly charged lattice with narrow pores, simulations were performed with and without explicit many-body polarization[20−23] contributions, in contrast to most extant molecular simulations. Molecular hydrogen's attractive interactions in a heterogeneous condensed phase matrix (e.g., MOFs, carbon nanostructures, and zeolites) are dominated by three intermolecular contributions: Van der Waals, charge-quadrupole, and induction. As an estimate of the relative importance of quadrupole (that are typically accounted for) and polarization (usually neglected) terms, consider a polarizable site with a point quadrupole, both of the magnitude appropriate for molecular hydrogen placed 0.30 nm distant from a double-charged cation (representing, e.g., indium in a charge state similar to that in *soc*-MOF). Given the most favorable geometry for the quadrupolar interactions, the polarization energy is a factor of 4 larger and is always attractive. Clearly, polarization is not negligible and needs to be included in some fashion. Below, we demonstrate that including many-body polarization explicitly has a dramatic effect on the physisorption of hydrogen to *soc*-MOF, even compared to explicitly including induction as a one-body interaction.

Further, these observations suggest that polarization needs to be included in modeling hydrogen sorption in a variety of materials, essentially because the quadrupole interactions are relatively weak. Note, ab initio molecular dynamics (MD) simulations of molecular hydrogen in another MOF (MOF-5) have been previously performed[24] and implicitly include a reasonably accurate representation of polarization interactions. Unfortunately, the high cost of performing ab initio MD simulations limits such finite temperature investigations to very short times, although they are quite effective at finding minimum energy configurations.

The rest of the paper is organized as follows. Section II A presents the parametrization and presentation of the hydrogen and *soc*-MOF energy function. Section II B presents the many-body polarization methods. Section II C and the Supporting

(16) Long, J. R.; Alivisatos, A. P.; Cohen, M. L.; Frechet, J. M. J.; Head-Gordon, M.; Louie, S. G.; Zettl, A.; Richardson, T. J.; Mao, S. S.; Read, C.; Alkire, J. *VI.D.2. A Synergistic Approach to the Development of New Classes of Hydrogen Storage Materials;* FY 2005 Progress Report; DOE Hydrogen Program; Department of Energy: Washington, DC, 2005.
(17) Abram, G.; Treinish, L. *Proc. IEEE Comp. Soc.* **1995**, *95*, 263.
(18) Haber, R.; Lucas, B.; Collins, N. *Proc. IEEE Vis.* **1991**, pp. 298−305.
(19) Lucas, B.; Abram, G. D.; Collins, N. S.; Epstein, D.; Gresh, D. and McAuliffe, K. *Proc. IEEE Vis.* **1992**, *92*, 107.
(20) Applequist, J.; Carl, J. R.; Fung, K.-K. *J. Am. Chem. Soc.* **1972**, *94*, 2952.
(21) van Duijnen, P. T.; Swart, M. *J. Phys. Chem. A* **1998**, *102*, 2399.
(22) Perry, A.; Neipert, C.; Moore, P.; Space, B. *Chem. Rev.* **2006**, *106*, 1234.
(23) Thole, B. *Chem. Phys.* **1981**, *59*, 341.
(24) Mulder, F.; Dingemans, T.; Wagemaker, M.; Kearley, G. *Chem. Phys.* **2005**, *317*, 113.

Information present the Monte Carlo methods. Section III presents the results of our simulations, and section IV reports the conclusions drawn from our studies.

II. Models and Methods

A. Molecular Simulation Parameters. A variety of theoretical methodologies have been used to study hydrogen sorption in nanostructured materials.[25−28] Recent studies include MD, grand-canonical Monte Carlo simulations to permit calculation of sorption isotherms, electronic structure studies to investigate binding mechanisms/affinities, and semiclassical simulations that differentiate the interaction of ortho and para hydrogen with a material (relevant at very low temperatures where neutron diffraction studies are performed to characterize underlying hydrogen interaction sites).[10,24,26−51]

Here, classical Monte Carlo simulation methods were chosen to study *soc*-MOF to perform equilibrium finite temperature simulations and to be able to explicitly study the role of induction in hydrogen sorption. Note, a recent study modeling hydrogen sorption in MOF materials[10] has shown that, under the relatively low-temperature conditions studied here, a quantum statistical mechanical description of the hydrogen structure is required to obtain quantitative accuracy. The earlier work included nuclear quantum dispersion effects via the computationally intensive path integral Monte Carlo simulations (PIMC), but did not include electronic induction. The results showed a decreased sorption of 10−15% relative to the purely classical simulations. However, that study also showed that the uncertainties in the Born−Oppenheimer potential surface were the dominant source of error in the simulations. Given that it is computationally prohibitive to perform PIMC simulations including polarization, the present study will focus on the role of electronic polarization within a classical model. Given the prior work, our estimates of hydrogen sorption strength may be a slight overestimate and the present work will focus on the critical role that polarization plays in shaping the Born−Oppenheimer surface. Including quantum dispersion effects will be the subject of future investigations.

Critical to any classical simulation based on empirical potentials is the careful selection of force field parameters. A minimal, yet effective, force field needs to include electrostatic, repulsive, and van der Waals-type interactions;[52,53] accurately describing the total potential energy surface is essential and the relevant parameters are not especially well-characterized for MOFs. Thus, striving for simplicity in this initial study, the need for framework intramolecular interactions was avoided by holding the scaffold rigid during simulation. Phonons are not thought to play an important role in hydrogen sorption, especially not at the temperatures considered here.[25] Lennard-Jones parameters, representing repulsive and van der Waals interactions between hydrogen atoms and framework were taken from the universal force field (UFF);[54] this set of parameters was used in earlier MOF studies.[10,27,34,38] The UFF interactions are parametrized for energetics between like atoms and all other interactions are accounted for in a standard way using (the approximate) Lorentz−Berthelot mixing rules.[52,54]

When neglecting polarizability, electrostatic interactions in atomistic simulations stem from point (partial) charges assigned to the coordinate corresponding to the nuclear center of each atom. Since the true electrostatic potential energy surface of *soc*-MOF is unknown and ab initio calculations on the *soc*-MOF unit cell are computationally prohibitive, point charges were determined from electronic structure calculations on several model compounds that mimic the chemical environment of the MOF atoms.[27] The GAMESS ab initio simulation package was used to perform the Hartree−Fock quantum mechanical calculations.[55]

The structure of *soc*-MOF is characterized by corner-sharing octahedral indium trimers joined by bent 1,3-benzenedicarboxylate organic linkers. Three representative fragments are shown in Figure 2. They all produced similar partial charges to within 10% on average, and the electrostatic parameters used were derived from the largest of the candidates: the results are presented in Table 1.

Study of the lattice shown in Figure 1 reveals the repetition of certain structures in a variety of geometries within the unit cell (for a detailed discussion of the structure see the literature).[11] The 448 atom unit cell may be produced from crystallographic symmetry operations from only twenty atoms.[11,14] Although this type of symmetry cannot be taken advantage of by quantum simulation packages, this repetition was used as a basis for deciding on representative chemical fragments. The largest fragments were chosen to include at least one complete metal center and an azobenzene linker; the smallest is the lone SBU. Adding hydrogen atoms where appropriate was required for chemical termination of the fragment boundaries. Measurements from the crystal structure indicate that the environments of the azobenzene linkers are essentially chemically equivalent in that their interface with the metal centers differs very slightly. Defining the azobenzene linkers as all chemically equivalent allows the entire unit cell to be defined in terms of only thirteen chemically different atoms. Using the electrostatic potential surface from the ab initio calculations, atomic point charges were fit using a standard algorithm.[55,56]

Since *soc*-MOF and our model fragments contain many-electron metal atoms (indium), the inner electrons require treatment via relativistic methods. Here we use semirelativistic pseudopotentials, and two were compared, namely SBKJC and LANL2[57−59] that include a different number of explicit electrons for indium (36 and 12, respectively) but gave similar results. The light atoms were treated at the 6-31G* level that produces over-polarized charges appropriate for condensed phase simulations (to account, in an

(25) Demontis, P.; Suffritti, G. B. *Chem. Rev.* **1997**, *97*, 2845.
(26) Froudakis, G. E. *J. Phys. Condens. Matter* **2002**, *14*, R453.
(27) Sagara, T.; Klassen, J.; Ganz, E. *J. Chem. Phys.* **2004**, *121*, 12543.
(28) Wang, Q.; Johnson, J. K. *J. Phys. Chem. B* **1999**, *103*, 4809.
(29) Bordiga, S.; Vitillo, J. G.; Ricchiardi, G.; Regli, L.; Cocina, D.; Zecchina, A.; Arstad, B.; Bjorgen, M.; Hafizovic, J. and Lillerud, K. P. *J. Phys. Chem. B* **2005**, *109*, 18237.
(30) Coker, D. F.; Berne, B. J. *J. Chem. Phys.* **1988**, *89*, 2128.
(31) Coker, D. F.; Thirumalai, D.; Berne, B. J. *J. Chem. Phys.* **1987**, *86*, 5689.
(32) Darkrim, F.; Levesque, D. *J. Chem. Phys.* **1998**, *109*, 4981.
(33) Darkrim, F. L.; Makbrunot, P.; Tartaglia, G. P. *Int. J. Hydrogen Energy* **2002**, *27*, 193.
(34) Duren, T.; Sarkisov, L.; Yaghi, O. M.; Snurr, R. Q. *Langmuir* **2004**, *20*, 2683.
(35) Fu, Q.; Negro, E.; Chen, G.; Law, D. C.; Li, C. H.; Hicks, R. F.; Raghavachari, K. *Phys. Rev. B* **2002**, *65*, 0753181.
(36) Hwang, D.-Y.; Mebel, A. M. *Chem. Phys. Lett.* **2000**, *321*, 95.
(37) Jhi, S.-H. *Microporous Mesoporous Mater.* **2006**, *89*, 138.
(38) Kawakami, T.; Takamizawa, S.; Kitagawa, Y.; Maruta, T.; Mori, W.; Yamaguchi, K. *Polyhedron* **2001**, *20*, 1197.
(39) Lee, S. M.; Lee, Y. H. *App. Phys. Lett.* **2000**, *76*, 2877.
(40) Mueller, T.; Cedar, G. *J. Phys. Chem. B* **2005**, *109*, 17974.
(41) Parrinello, M.; Rahman, A. *J. Chem. Phys.* **1984**, *80*, 860.
(42) Schlapbach, L.; Zuttel, A. *Nature* **2001**, *414*, 353.
(43) Shirono, K.; Endo, A.; Daiguji, H. *J. Phys. Chem. B* **2005**, *109*, 3446.
(44) Simonyan, V. V.; Diep, P.; Johnson, J. K. *J. Chem. Phys.* **1999**, *111*, 9778.
(45) Sun, Q.; Wang, Q.; Jena, P.; Kawazoe, Y. *J. Am. Chem. Soc.* **2005**, *127*, 14582.
(46) Wang, Q.; Johnson, J. K. *J. Phys. Chem. B* **1999**, *103*, 277.
(47) Wang, Q.; Johnson, J. K. *J. Chem. Phys.* **1999**, *110*, 577.
(48) Yang, Q.; Zhong, C. *Phys. Chem. B* **2006**, *110*, 655.
(49) Zidan, R. A.; Rocheleau, R. E. *J. Mater. Res.* **1999**, *14*, 286.
(50) MacKinnon, J. A.; Eckert, J.; Coker, D. F.; Bug, A. L. *J. Chem. Phys.* **2001**, *114*, 10137.
(51) Larin, A.; Cohen De Lara, E. *J. Chem. Phys.* **1994**, *101*, 8130.
(52) Allen, M. P.; Tildesley, D. J. *Computer Simulation of Liquids*; Clarendon Press: Oxford, England 1989.
(53) Frenkel, D.; Smit, B. *Understanding Molecular Simulation: From Algorithms to Applications;* Academic Press: New York, 2002.
(54) Rappe, A.; Casewit, C.; Colwell, K.; Goddard, W., III; Skiff, W. *J. Am. Chem. Soc.* **1992**, *114*, 10024.
(55) Schmidt, M. W.; Baldridge, K. K.; Boatz, J. A.; Elbert, S. T.; Gordon, M. S.; Jensen, J. H.; Koseki, S.; Matsunaga, N.; Nguyen, K. A.; Su, S.; Windus, T. L.; Dupuis, M.; Montgomery, J. A. *J. Comput. Chem.* **1993**, *14*, 1347.
(56) Singh, U.; Kollman, P. *J. Comput. Chem.* **1984**, *5*, 129.
(57) Hay, P. J.; Wadt, W. R. *J. Chem. Phys.* **1985**, *82*, 270.
(58) LaJohn, L. A.; Christiansen, P. A.; Ross, R. B.; Atashroo, T.; Ermler, W. C. *J. Chem. Phys.* **1987**, *87*, 2812.
(59) Stevens, W. J.; Basch, H.; Krauss, M. *J. Chem. Phys.* **1984**, *81*, 6026.

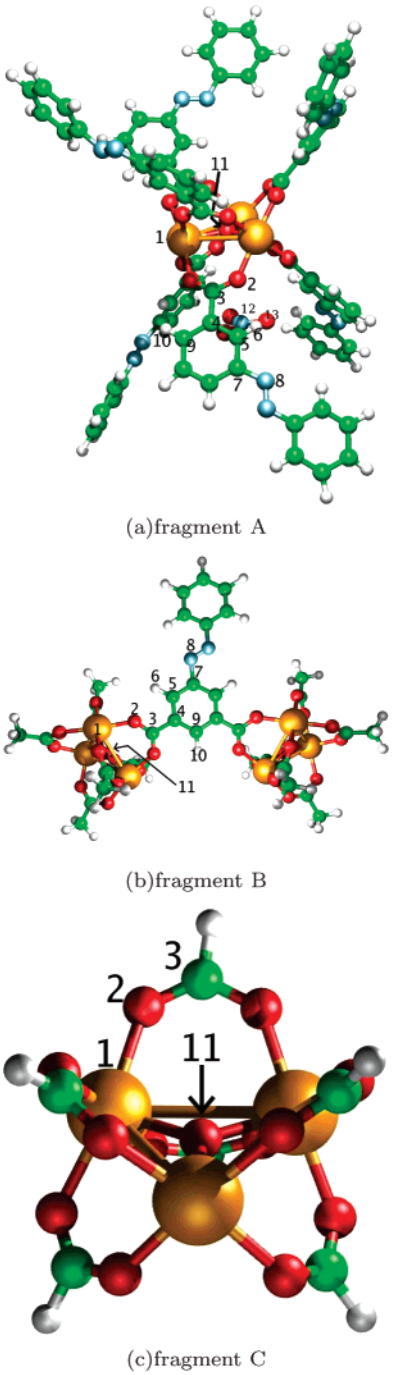

Figure 2. Illustrations depicting the fragments used in the ab initio calculation of the partial charges. Structure A is an SBU with six bound linkers, essentially one complete corner of a pore. Structure B, two SBUs coupled by one linker, can be regarded as the edge of a pore. Structure C is essentially the bare SBU used in the design of *soc*-MOF[11]. Note that for clarity, the nitrate anions are not depicted in fragments B and C of the figure (but they were included in all calculations).

effective way, for the effect of self-induction of the unpopulated lattice).[60] As a further test of the ab initio calculations, relativistic electronic structure calculations were performed on the smallest fragment (without need for pseudopotentials) using a third-order Douglas−Kroll transformation and the corresponding DK3 basis set.[61]

Table 1. Partial Charges Taken from the Fragment (Figure **2a**) Used in Simulation of *soc*-MOF

atom	label	charge (e$^-$)
In	1	2.0697
O	2	−0.7588
C	3	0.9108
C	4	−0.1086
C	5	−0.2252
H	6	0.1366
C	7	0.3785
N	8	−0.2243
C	9	−0.1327
H	10	0.2167
O	11	−1.3978
N (nitrate)	12	0.6934
O (nitrate)	13	−0.4652

Table 2. Partial Charges for the Fragment in Figure **2b** for Comparison

atom	label	charge (e$^-$)
In	1	2.228
O	2	−0.8216
C	3	0.9652
C	4	−0.1286
C	5	−0.2622
H	6	0.1443
C	7	0.4631
N	8	−0.2111
C	9	−0.2150
H	10	0.1854
O	11	−1.5424
N (nitrate)	12	1.029
O (nitrate)	13	−0.6424

The resulting charges agreed within 7.0% of those used in this study; the charges used herein are tabulated in Table 2. Note that the condensed phase polarization of the neat MOF is included implicitly, while the polarization interactions in our simulations between the hydrogen and the MOF will be treated explicitly.

Partial charges for hydrogen were chosen to reproduce the quadrupole moment of the molecule.[32] The hydrogen is also treated as rigid and its high-frequency vibration is not expected to contribute to sorption.[32] The electrostatic model is a three-point model with a charge located at the center of mass. The hydrogen atoms are separated by 0.741 Å and interact (between distinct molecules) via a polarizable many-body potential, along with the Coulombic and UFF-defined Lennard-Jones intermolecular pair potentials.

B. Polarizability Model. Molecular polarization was explicitly included in the Monte Carlo simulations by use of the Thole−Applequist model.[20,21,23] This model treats the system in terms of site (atomic) point dipoles that interact via many-body polarization equations. Once atomic point polarizabilities are fit to a training set of molecules the model has been shown to accurately reproduce molecular/system dipoles in a transferable (i.e., system-independent) manner.[20,21] This model of explicit polarization has been successfully applied in numerous areas where inclusion of polarizable effects is paramount, such as vibrational spectroscopy,[22,62,63] liquid dynamics,[64−67] and biomolecules.[68,69]

(60) Cornell, W. D.; Cieplak, P.; Bayly, C. I.; Gould, I. R.; Kenneth, J.; Merz, M.; Ferguson, D. M.; Spellmeyer, D. C.; Fox, T.; Caldwell, J. W.; Kollman, P. A. *J. Am. Chem. Soc.* **1995**, *117*, 5179.
(61) Tsuchiya, T.; Abe, M.; Nakajima, T.; Hirao, K. *J. Chem. Phys.* **2001**, *115*, 4463.
(62) Applequist, J.; Quicksall, C. O. *J. Chem. Phys.* **1977**, *66*, 3455.
(63) DeVane, R.; Space, B.; Perry, A.; Neipert, C.; Ridley, C.; Keyes, T. *J. Chem. Phys.* **2004**, *121*, 3688.
(64) Bernardo, D. N.; Ding, Y.; Krogh-Jespersen, K.; Levy, R. M. *J. Phys. Chem.* **1994**, *98*, 4180.
(65) Christian, S. S. X.; Burnham, J.; Jichen, L.; Leslie, M. *J. Chem. Phys.* **1999**, *110*, 4566.
(66) Ren, P.; Ponder, J. W. *J. Phys. Chem. B* **2003**, *107*, 5933.
(67) Souaille, M.; Smith, J. C. *Mol. Phys.* **1996**, *87*, 1333.
(68) Bode, K. A.; Applequist, J. *J. Phys. Chem.* **1996**, *100*, 17825.
(69) Ren, P.; Ponder, J. W. *J. Comput. Chem.* **2002**, *23*, 1497.

Consider a static electric field applied to a molecule. The induced dipole on this molecule will be equal to

$$\vec{\mu}_{\mathrm{mol}} = \boldsymbol{\alpha}_{\mathbf{mol}} \boldsymbol{E}^{\mathrm{stat}} \tag{1}$$

where $\boldsymbol{\alpha}_{\mathbf{mol}}$ is the 3×3 molecular polarizability tensor unique to that molecule. We now consider the molecular dipole as being a sum of atomic point dipoles, one for each atom of the molecule. If we label each atomic point dipole vector $\vec{\mu}_i$ then we have

$$\vec{\mu}_i = \boldsymbol{\alpha}_i \vec{E}_i^{\mathrm{stat}}$$

$$\vec{\mu}_{mol} = \sum_i^N \vec{\mu}_i \tag{2}$$

where $\boldsymbol{\alpha}_i$ is the 3×3 site polarizability tensor and $\vec{E}_i^{\mathrm{stat}}$ is the electrostatic field at the site. In the Thole−Applequist model the system is treated as a collection of N dipoles along with a dipole field tensor $\mathbf{T}_{ij}^{\alpha\beta}$ which contains the complete set of induced dipole−dipole interactions. This dipole field tensor, when contracted with the system dipoles, yields the (many-body) induced-dipole contribution to the electric field—this contribution is denoted here as $\vec{E}^{\mathrm{ind}}$. Since the dipole field tensor (by construction) contains the entire induction contribution, we can assign a *scalar* point polarizability, α_i°, to each site rather than a polarizability tensor:

$$\mu_i = \alpha_i^\circ (\vec{E}_i^{\mathrm{stat}} + \vec{E}_i^{\mathrm{ind}}) \tag{3}$$

$$= \alpha_i^\circ (\vec{E}_i^{\mathrm{stat}} - \mathbf{T}_{ij}^{\alpha\beta} \vec{\mu}_j) \tag{4}$$

This equivalence can be demonstrated by reproducing the site polarizability tensors via

$$\mathbf{A}\vec{\mu} = \vec{E}^{\mathrm{stat}} \tag{5}$$

$$\vec{\mu} = \mathbf{B}\vec{E}^{\mathrm{stat}} \tag{6}$$

where $\vec{\mu}$ and $\vec{E}^{\mathrm{stat}}$ are supervectors formed by stacking the system dipole/field vectors:

$$\vec{\mu} = \begin{pmatrix} \vec{\mu}_1 \\ \vec{\mu}_2 \\ \vec{\mu}_3 \\ \bullet \\ \bullet \\ \bullet \\ \vec{\mu}_N \end{pmatrix}$$

$$\vec{E}^{\mathrm{stat}} = \begin{pmatrix} \vec{E}_1^{\mathrm{stat}} \\ \vec{E}_2^{\mathrm{stat}} \\ \vec{E}_3^{\mathrm{stat}} \\ \bullet \\ \bullet \\ \bullet \\ \vec{E}_N^{\mathrm{stat}} \end{pmatrix}$$

and the matrices $\mathbf{A}$ and $\mathbf{B}$ are defined by

$$\mathbf{A} = [(\alpha^\circ)^{-1} + \mathbf{T}_{ij}^{\alpha\beta}] \tag{7}$$

$$\mathbf{B} = A^{-1}$$

Just as $\mathbf{A}$ is a supermatrix composed of 3×3 block elements $\mathbf{T}_{ij}$, $\mathbf{B}$ can be decomposed as[21]

$$\mathbf{B} = \begin{pmatrix} \mathbf{B}_{11} & \mathbf{B}_{12} & \bullet & \mathbf{B}_{1N} \\ \mathbf{B}_{21} & \mathbf{B}_{22} & \bullet & \bullet \\ \bullet & \bullet & \bullet & \bullet \\ \mathbf{B}_{N1} & \bullet & \bullet & \mathbf{B}_{NN} \end{pmatrix}$$

where each block element $\mathbf{B}_{ij}$ is a 3×3 matrix. These block elements $\mathbf{B}_{ij}$ are the site polarizability tensors and thus characterize the site's response to an electric field. For example, the matrix $\mathbf{B}_\eta$ formed by summing the ηth row of $\mathbf{B}$

$$\mathbf{B}_\eta = (\mathbf{B}_{\eta 1} + \mathbf{B}_{\eta 2} + ... + \mathbf{B}_{\eta N})$$

determines the dipole response to a field for site η as a function of all N sites since (making use of eq 6)

$$\vec{\mu}_\eta = \mathbf{B}_{\eta 1}\vec{E}_1^{\mathrm{stat}} + \mathbf{B}_{\eta 2}\vec{E}_2^{\mathrm{stat}} + ... + \mathbf{B}_{\eta N}\vec{E}_N^{\mathrm{stat}}$$

$$= \vec{\mu}_\eta(1) + \vec{\mu}_\eta(2) + ... + \vec{\mu}_\eta(N)$$

whereby each μ term represents a contribution toward η's dipole. Therefore, summing all of the ij blocks over the tensor components $\alpha\beta$ for an appropriate set of sites yields the molecular polarizability tensor:[21]

$$\boldsymbol{\alpha}_{\alpha\beta}^{\mathrm{mol}} = \sum_{ij} (\mathbf{B}_{ij})_{\alpha\beta} \tag{8}$$

The Applequist dipole field tensor[20] can be derived from first principles as

$$\mathbf{T}_{ij}^{\alpha\beta} = \nabla_\alpha \nabla_\beta \frac{1}{r_{ij}}$$

$$= \frac{\delta_{\alpha\beta}}{r_{ij}^3} - \frac{3x^\alpha x^\beta}{r_{ij}^5} \tag{9}$$

The most direct way to calculate the system dipoles is through eq 6. However, since inversion of the $3N \times 3N$ matrix $\mathbf{A}$ is computationally efficient for only the smallest systems, the dipoles must be solved for by an iterative method. The iterative method employed here makes an initial guess of $\vec{\mu}_i = \alpha_i^\circ \cdot \vec{E}_i^{\mathrm{stat}}$ and then iteratively solves eq 4 until convergence is achieved.

The Thole model introduces the additional consideration of treating each dipole as interacting with a well-behaved charge distribution $\rho(u)$ (in contrast to the Applequist model where the dipole field tensor is derived by considering a dipole interacting with a point charge, giving rise to eq 9), which results in a modified form of the dipole field tensor. The net result of this modification is that the charge which induces each dipole is "smeared" at short range, and it is this additional structure that Thole added to the model which imparts transferability. One such exponential distribution[23] found to accurately and transferably[21] reproduce molecular dipoles for an associated series of dependent polarizabilities is

$$\rho(u_{ij}) = \frac{\lambda^3}{8\pi} \mathrm{e}^{-\lambda u_{ij}}$$

$$u_{ij} = x_{ij}(\alpha_i^\circ \alpha_j^\circ)^{-(1/6)} \tag{10}$$

where the free parameter λ has the effect of damping the dipole interactions near the regions of discontinuity that would otherwise exist in the Applequist model. The coordinate scaling of $x_{ij} \rightarrow u_{ij}$ is done for convenience to allow simple functional forms such as eq 10 to be used for damping. Taking the exponential charge distribution into account, the modified dipole field tensor becomes[21]

$$\hat{T}_{ij}^{\alpha\beta} = \frac{\delta_{\alpha\beta}}{r_{ij}^3}\left[1 - \left(\frac{\lambda^2 r_{ij}^2}{2} + \lambda r_{ij} + 1\right) e^{-\lambda r_{ij}}\right] - \frac{3x^\alpha x^\beta}{r_{ij}^5}\left[1 - \left(\frac{\lambda^3 r_{ij}^3}{6} + \frac{\lambda^2 r_{ij}^2}{2} + \lambda r_{ij} + 1\right) e^{-\lambda r_{ij}}\right] \quad (11)$$

The many-body potential energy due to the interaction of the induced dipoles (referred to as the polarization energy) is described by[23]

$$U_{\text{pol}} = \sum_i \frac{1}{2}\vec{\mu}_i \cdot \mathbf{A}\vec{\mu}_i - \vec{\mu}_i \cdot \vec{E}_i^{\text{stat}} = \sum_i \frac{1}{2}\vec{\mu}_i \cdot \vec{E}_i^{\text{stat}} - \vec{\mu}_i \cdot \vec{E}_i^{\text{stat}} = -\frac{1}{2}\sum_i \vec{\mu}_i \cdot \vec{E}_i^{\text{stat}} \quad (12)$$

where it should be pointed out that $\vec{E}_i^{\text{stat}}$ is not the total electric field, but rather only the static electric field due to the presence of the partial charges present in the system.

Calculating the polarization energy for the system amounts to self-consistently solving the dipole field equation for each atomic dipole vector $\vec{\mu}_i$ through an iterative process until a sufficient degree of precision is achieved. Thus, to make the calculations practical, efficient methods of solving the field equations were required. Typically, a simultaneous over-relaxation scheme (i.e., linear solution mixing) is used to improve the convergence rate for the iterative method of solution.[65] However, recently a number of multigrid techniques[70] have been applied to the Thole model for a one-dimensional system,[71] and a similar Gauss−Seidel smoothing technique was applied here and found to reduce the number of iterations required for convergence by 2-fold over linear mixing. The applied Gauss−Seidel numerical iteration method for a slowly converging process consists of updating the current dipole vector set for the *k*th iteration step as the new dipole vectors become available:

$$\vec{\mu}_i^k = \alpha_i^\circ(\vec{E}_i^{\text{stat}} - \hat{T}_{ij}^{\alpha\beta}\vec{\mu}_j^{k-1+\zeta}) \quad (13)$$

$$\zeta = \begin{cases} 0, & \text{if } i < j \\ 1, & \text{if } i > j \end{cases}$$

Dipoles were calculated to a precision of 10^{-4} Debye and were subject to a 11.2 Å (half the unit cell length) spherical cutoff. Since the atomic point charges of the MOF were calculated by ab initio to implicitly include polarization, MOF−MOF self-polarization was disallowed by excluding MOF−MOF electric field interactions, and only the induced field interactions between the H_2 and MOF atoms were calculated. All system dipoles were allowed to interact through the exponentially damped dipole field tensor (given by eq 11) subject to the constraint of the spherical cutoff.

The polarizability tensor of diatomic hydrogen with an equilibrium bond distance of 0.741 Å was calculated by the restricted Hartree−Fock method with a correlation-consistent double-ζ basis set[72] (augcc-pVDZ) using GAMESS.[55] The atomic Thole polarizabilities for molecular hydrogen were then determined by fitting α^{mol} to the HF polarizability tensor form while at the same time yielding one-third of the trace equal to the experimentally measured[73] H_2 polarizability of 0.787 Å^3; the values that best satisfied both criteria were found to be 0.2658 Å^3 for H and 0.5865 Å^3 for the center of mass site.

The SBU of *soc*-MOF contains indium which, in complex, has a partial charge of about In^{2+} as fit to the calculated electrostatic potential surface of the gas-phase fragment (see Table 1). While the polarizability of closed shell indium is known,[74] the polarizability of indium in the 2+ state has not been parametrized previously for the Thole model, nor has it been experimentally elucidated. To ascertain the polarizability, ab initio simulations were performed using finite-field calculations on In^0, In^{1+}, In^{2+}, and In^{3+} . To ensure that the results obtained from the finite-field calculations were reasonable the data was compared to polarizabilities calculated with an analytic Hessian for the In^{1+} and In^{3+} states. Thus an estimate of 2.0 Å^3 for In^{2+} was determined for these results; future research will be directed at applying fully relativistic field equations to the SBU and fitting this parameter within the Thole model. The remainder of the MOF atoms were given the exponential polarizabilities and associated damping parameter as calculated by van Duijnen et al.[21]

C. NVT Monte Carlo. Monte Carlo[75] simulations were performed on the H_2-MOF system at 78 K and with the experimentally determined hydrogen density of 113 molecules per unit cell,[11] with periodic boundary conditions applied. The total potential for the system is described by

$$U = U_{\text{elect}} + U_{\text{pol}} + U_{\text{LJ}} \quad (14)$$

where U_{elect} is the electrostatic potential energy calculated from the Ewald field, U_{pol} is the polarization energy calculated from eq 12, and U_{LJ} is the Lennard-Jones potential.

Monte Carlo moves were made by selecting an H_2 molecule at random and performing a random rigid-body translation and rotation of the molecule. The MC move was then accepted or rejected according to the Metropolis function:

$$\min(1, e^{-\beta\Delta U}) \quad (15)$$

Using simple Monte Carlo moves is not especially desirable given the need to entirely reevalulate the many-body polarization energy after each small move. In an attempt to make global moves that would more efficiently explore phase space, several hybrid Monte Carlo schemes[76,77] were implemented with forces that were computed from the nonpolarizable potential. Unfortunately, the potential-energy surfaces are sufficiently dissimilar and the approach failed; this result, however, was also an indication of the essential role of polarization interactions in this system. The details of the hybrid Monte Carlo implementation are given in the Supporting Information.

The Monte Carlo algorithm and many-body polarization code were implemented within a package originally developed by the Klein group at the Center for Molecular Modeling at the University of Pennsylvania.[78−81] A cellular automata-based (rule 30) pseudorandom number generator was implemented for its superior random number quality.[82,83] The magnitude of the MC moves were adjusted to yield a 25% acceptance rate to minimize the correlation time. Autocorrelation of the polarization energy gave a correlation time of $\tau = 25000$ Monte Carlo steps. After

(70) Griebel, M.; Keyes, D.; Nieminen, R.; Roose, D.; Schlick, T. *Discretization Methods and Iterative Solvers Based on Domain Decomposition, Lecture Notes in Computational Science and Engineering;* Springer: Berlin, 2001).
(71) Dinh, T.; Huber, G. A.; Math, J. *Modell. Algorithms* **2005**, *4*, 111.
(72) Dunning, T. H., Jr. *J. Chem. Phys.* **1989**, *90*, 1007.
(73) Computational Chemistry Comparison and Benchmark Database. http://srdata.nist.gov/cccbdb, released Aug 12, 2005 (accessed 2006).
(74) Guella, T.; Miller, T. M.; Bederson, B.; Stockdale, J.; Jaduszliwer, B. *Phys. Rev. A* **1984**, *29*, 2977.
(75) Metropolis, N.; Rosenbluth, A. W.; Rosenbluth, M. N.; Teller, A. H.; Teller, E. *Phys. Lett. B* **1953**, *21*, 1087.
(76) Duane, S.; Kennedy, A.; Pendleton, B. J.; Roweth, D. *Phys. Lett. B* **1987**, *195*, 216.
(77) Mehlig, B.; Heermann, D.; Forrest, B. *Phys. Rev. B* **1992**, *45*, 679.
(78) Moore, P.; Lopez, C. F.; Klein, M. L. *Biophys. J.* **2001**, *81*, 2484−2494.
(79) Moore, P.; Zhong, Q.; Husslein, T.; Klein, M. L. *FEBS Lett.* **1998**, *431*, 143−148.
(80) Tarek, M.; Tu, K.; Klein, M. L.; Tobias, D. J. *Biophys. J.* **1999**, *77*, 964−972.
(81) Zhong, Q.; Moore, P. B.; Klein, M. L. *FEBS Lett.* **1998**, *427*, 267−274.
(82) Wolfram, S. *Rev. Mod. Phys.* **1983**, *55*, 601.
(83) Wolfram, S. *A New Kind of Science*; Wolfram Media: Champaign, IL, 2002.

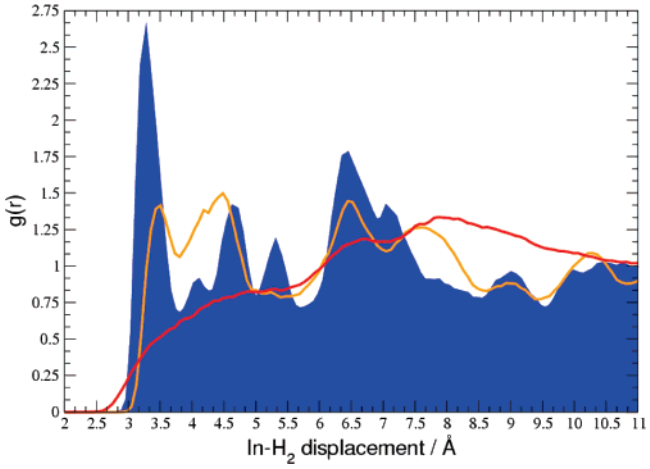

Figure 3. Radial distribution functions between the center of mass for the hydrogen to the indium under experimental conditions for three different potentials: Thole−Applequist many-body polarizable potential (blue), nonpolarizable potential (orange), and Lennard-Jones only (red).

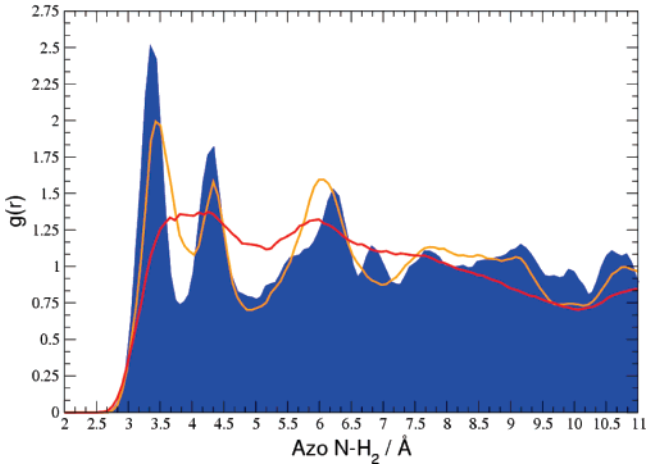

Figure 4. Radial distribution functions between the center of mass for the hydrogen to the azo nitrogen under experimental conditions for three different potentials: Thole−Applequist many-body polarizable potential (blue), nonpolarizable potential (orange), and Lennard-Jones only (red).

a system equilibration time of 500 000 steps, atomic configurations and system dipoles were then sampled at intervals of 2τ for the collection of uncorrelated states of H_2 in the MOF. A total of 17.5 million MC steps were calculated on the massively parallel supercomputer LoneStar (Teragrid/University of Texas at Austin) to sample 350 uncorrelated configurations from the canonical ensemble.

Nonpolarizable MC runs, calculating only the electrostatic and LJ terms in eq 14, were also enacted for comparison. The magnitude of trial movement was able to be greatly increased and the potential energy correlation time was $\tau = 2500$ MC steps—an order of magnitude less than that of the polarized system. Clearly, inclusion of the many-body polarizable potential greatly decreases the efficiency of the MC technique (when making simple one-body trial moves) *in addition to* the computational overhead introduced by the Thole model; the calculation of the system dipoles consumes approximately 95% of the total CPU time. However, the computational cost is still far below that of performing ab initio dynamics.

The radial distribution function $g(r)$ was calculated between the hydrogen and various sites on the MOF and error analysis was performed to ensure their convergence. Isosurface analysis was performed over both the hydrogen population density and the hydrogen dipole magnitude.

III. Results and Discussion

To demonstrate the effect of polarization on sorption in *soc*-MOF, Figure 3 shows the radial distribution function between the sorbed hydrogen and indium ions both when induction is included and neglected. The polarization interactions strongly influence the structure of the sorbed hydrogen in the region of the metal ions. The figure also shows the distribution function when both charge-quadrupole and induction effects are neglected; in this case hydrogen is interacting as a Lennard-Jones species with the MOF framework. Thus, the charge-quadrupole interactions are also making an important contribution to the sorption structure. While the effect is less dramatic, the radial distribution function shown in Figure 4 between the hydrogen and azobenzene nitrogen shows that the polarization effect of the azobenzene is also significant.

Further insight is gained by examining the distribution of H_2 induced dipoles that are produced by the field from the charges on the MOF (previous simulations in this study show that the contribution toward MOF polarization from the quadrupolar hydrogen−hydrogen interactions are negligible, yet, for completeness, they were also included here). Figure 5 plots the distribution of induced dipoles that is approximately a bimodal Gaussian distribution with a dominant low dipolar (78% of the population with a mean dipole 0.18 Debye) and high dipolar species (22% of the population with a mean dipole 0.33 Debye). Analysis of molecular dipole magnitude isosurfaces reveals that the low dipolar population corresponds to spatial regions localized in the vicinity of the open coordination sites of the SBUs (shown in Figure 6), while the high dipolar population is localized in the middle of the window formed by the azobenzene linkers. The reason for the high dipole distribution being associated with the azobenzene linkers seems to be because the location of the window is geometrically proximal to all of the dominantly charged structures, namely the indium complex, nitrate anion, and azo linkage. Enhancement of the first neighbor peak of the radial distribution function to the nitrogen of the azobenzene, shown in Figure 4, would seem to support this. The low dipolar population is associated with the electric field of the positively charged and highly polarizable indium ions of the SBU. The open coordination site of the indium also permits hydrogen to strongly associate with the metal ions as shown in Figure 1.

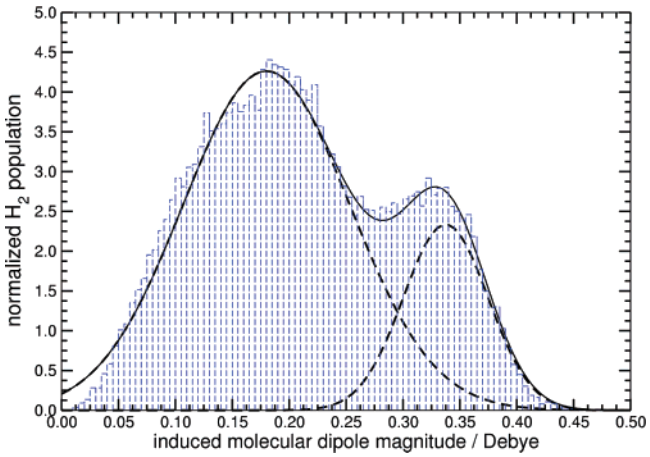

Figure 5. Bimodal H_2 molecular dipole magnitude distribution for *soc*-**MOF at 78 K under the experimental density. The figure presents a fit of the dipole distributions to two decomposed Gaussian distributions.**

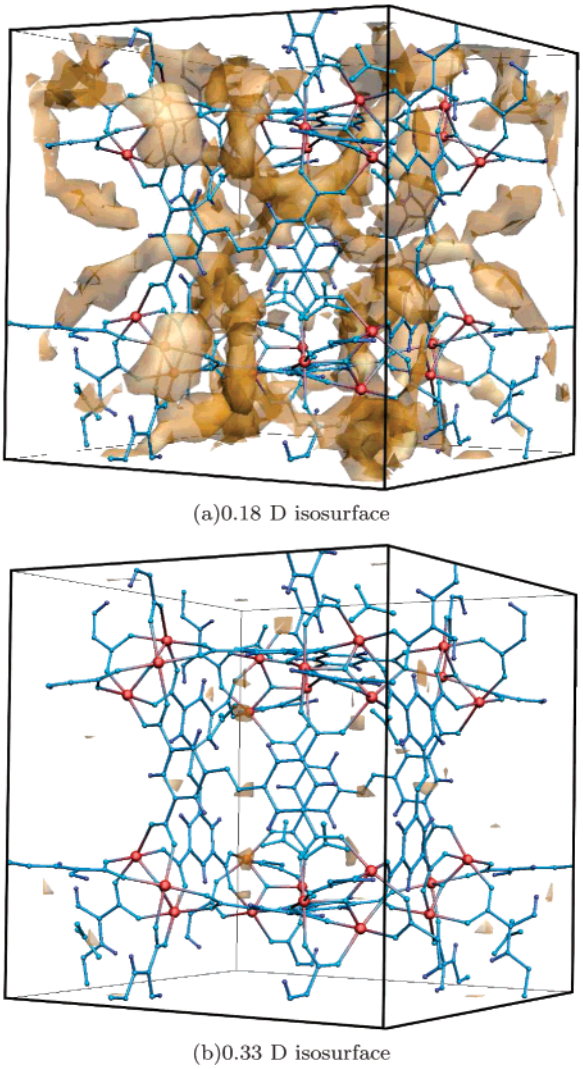

Figure 6. Isosurfaces showing the low-dipolar and high-dipolar hydrogen species corresponding to the respective peaks of the bimodal hydrogen dipole distribution. Note the location of the indium open coordination sites (red) and the nitrate anions (lower corners of the box most visible) with respect to the high-dipolar isosurface.

To put the magnitude of the dipoles in context, if we consider the hydrogen in the MOF a polar diatomic liquid with a dipole characteristic of the dominant species of 0.18 Debye, this magnitude is comparable to the permanent dipoles of NO (0.16 Debye) or CO (0.11 Debye) that have ambient boiling points of 121 and 82 K, respectively. Thus, while neat hydrogen at 78 K has a negligible induced dipole (and is essentially an ideal gas with $PV/NkT = 1.00$),[1] the hydrogen in the MOF experiences mutual, many-body, dipolar attractions. Thus, it is reasonable that it is nearly condensed in the MOF pores at the conditions considered here and in the experiment at 78 K.

To assess the importance of polarization effects in a MOF with a less polar framework, we used the same force-field parameters and charge-fitting protocols to develop a potential-energy surface for the much studied IRMOF-1 (aka MOF-5).[12] Simulations including many-body polarization for IRMOF-1 reveal no significant change in radial distribution functions for the hydrogen to the metal-centered SBU when compared to simulations neglecting induction. MOF-5, which sorbs substantially less hydrogen than the new material studied here under like conditions, also does not possess an open coordination site on its zinc SBU and thus produces a more weakly polarizing field in comparison with *soc*-MOF. Most importantly, MOF-5 does not possess narrow channels or a highly polar framework, but rather has an open topology with larger void spaces. This comparison strongly suggests that MOFs, like MOF-5, with large pores are not the best target materials for super-hydrogen-storage. *The key result of this study is that hydrogen needs to interact sufficiently strongly with a MOF to produce a dipolar fluid with a characteristically higher condensation temperature.*

Recently, hydrogen storage in a Mn-containing MOF was studied[84] in which a similar sorption isotherm as that of *soc*-MOF was measured; this MOF also possesses relatively narrow channels and a polar framework. This cubic topology MOF contains an Mn^{2+} open coordination site on the SBU; it is not unreasonable then to assume that the high sorption capacity of hydrogen in both that material and *soc*-MOF are correlated with the structural motif of the SBU. The dipole isosurfaces generated by this work would suggest that the open coordination sites serve to polarize the hydrogen under the experimental conditions.

Using the polarizable potential, the integral enthalpy of adsorption for the hydrogen in *soc*-MOF was calculated by

$$\Delta H^a = E(\mathrm{MOF} + \mathrm{H_2}) - [E(\mathrm{MOF}) + E(\mathrm{H_2})]$$

Note that the PV terms are negligible in this case. To be clear, the energy for the MOF with N hydrogen molecules present is calculated and then subtracted from the combined energy for the MOF alone and the neat gas of N hydrogen molecules; the energy is then divided by the number of moles corresponding to the N molecules. The integral enthalpy was calculated at both the saturated state (113 hydrogen molecules per unit cell) and the zero-loading limit (a single hydrogen molecule per unit cell).

It is important to note that this differs from the experimentally measured isosteric heat of adsorption, q_{st} in that we are calculating the integrated energy per mole of adsorbent. The numbers are expected to be very similar, however, for the following reasons: the isosteric heat is given by

$$q_{st} = kT^2 \frac{\partial \ln P}{\partial T}$$

while the differential enthalpy is equal to

$$\Delta h^a = kT^2 \frac{\partial \ln f}{\partial T}$$

where $f = \phi P$ is the fugacity and ϕ is the fugacity coefficient.[10,85,86] The condition for these quantities to be equal is that the temperature dependence of the fugacity coefficient is small, namely: $(1/\phi)(\partial\phi/\partial T) \ll (1/P)(\partial P/\partial T)$, a requirement that is clearly met under the sorptions conditions considered here where the hydrogen structure is not changing dramatically with temperature (note that even for an ideal gas, the $(\partial \ln P/\partial T)$ term has a strong $(1/T)$ dependence). To complete the argument, note (considering *soc*-MOF) there is a weak dependence on loading in the isosteric heat measurements,[11] and, in the limit that $q_{st} \approx \Delta h^a$ is constant, it is equal to the integral adsorption heat, making a comparison reasonable.[85,86]

(84) Dinca, M.; Dailly, A.; Liu, Y.; Brown, C. M.; Neumann, D. A.; Long, J. R. *J. Am. Chem. Soc.* **2006**, *128*, 16876.
(85) Meyers, A. *Am. Inst. Chem. Eng.* **2002**, *48*, 145.
(86) Meyers, A. L.; Siperstein, F. *Colloids Surf., A* **2001**, *73*, 187−188.

ΔH^a_{sat} was found to be -10.645 ± 0.188 kJ mol^{-1}, while the unsaturated state yielded ΔH^a_{unsat} of -14.354 ± 1.685 kJ mol^{-1}; the relatively constant ΔH^a values indicate the retention of strong attractive interactions even at higher loadings, which is also supported by the experimentally measured isosteric heats.[11] Polarization contributed 23% of the total potential energy at saturation and 27% when unsaturated. These enthalpies appear large compared to the experimental measurements that give a relatively constant isosteric heat of sorption of about 6.5 kJ mol^{-1}.[11] Thus, as a control, the integral heats of sorption in IRMOF-1 at the low-density limit were calculated to compare with existing experimental[12] and theoretical[10] values. The result was $\Delta H^a_{unsat} = -5.998 \pm 0.298$ kJ mol^{-1}, in good agreement with extant values. Including polarization gave a value of $\Delta H^a_{unsat} = -6.343 \pm 0.277$ kJ mol^{-1}, consistent with the result that including polarization in simulating saturated IRMOF-1 did not significantly change the hydrogen structure within the MOF. As was pointed out in a previous work[10] it is often difficult to say why there is a discrepancy between the experiment and theory in one case versus another,[10] but all of the evidence does clearly support that polarization is a critical factor influencing sorption in *soc*-MOF.

IV. Conclusions

The results of this study suggest desirable MOF design characteristics for hydrogen and gas storage in general—MOFs are promising candidates for gas storage/sequestration. For example, one would expect CO_2 sorption in *soc*-MOF to be quite strong given the significantly higher molecular quadrupole and polarizabilty. This study suggests that MOFs should have relatively small pores and interconnected pores with high surface area to create strong MOF$-H_2$ interactions and, thus, indirectly H_2-H_2 attractions. To promote these interactions, the MOF also needs to be locally polar with large charge separations on its surface sufficiently far apart to allow hydrogen molecules to be sensitive to the dipolar interface. Further, while the surface area needs to be large, the open spatial network should not be so expansive that hydrogen molecules farthest from the MOF surface do not possess significant induced dipoles and charge-quadrupole forces. For example, if a MOF were to possess a large surface area owing to sizable pores, hydrogen toward the center of the void will be similar to neat hydrogen with characteristically weak intermolecular interactions and a correspondingly lower condensation temperature. There is, however, a tradeoff between having larger voids that produce a lower molecular weight material (but do not promote strong sorptive forces) versus having a highly nanostructed pore system (with correspondingly more material per unit, but strong scaffold$-H_2$ interactions).

These initial studies have provided significant insights into the nature of hydrogen interactions in nanporous, polar MOF materials. The results presented also suggest several future avenues of inquiry. Foremost, we will proceed to calculate sorption isotherms for our model using a Widom insertion method[87−89] that can be compared with experiment. This will also serve to further calibrate the potential energy surface of our molecular mechanics model by, for example, giving us the system pressure at the experimentally observed hydrogen loading. We can then proceed to mutate the MOF in an experimentally plausible fashion in an attempt to increase its hydrogen storage capacity. Last, this study suggests that including polarization in modeling other extant and future MOFs can give reliable physical insight into the mechanism of gas storage.

Acknowledgment. The research at USF was supported by NSF Grant No. CHE-0312834 and a grant from the Petroleum Research Fund to Brian Space. The authors would like to acknowledge the use of the services provided by the Teragrid and the Research Computing Center at USF. The authors also thank the Space (Basic and Applied Research) Foundation for partial support. Mohamed Eddaoudi acknowledges funding from an NSF grant (No. DMR-0548117). Mohamed Eddaoudi and Brian Space acknowledge funding from NASA (Grant No. NGA3-2751) and the Department of Energy, Basic Energy Sciences (Grant No. DE0GG02-07ER46470). This material is based upon work supported by the National Science Foundation under the following NSF programs: Partnerships for Advanced Computational Infrastructure, Distributed Terascale Facility (DTF), and Terascale Extensions: Enhancements to the Extensible Terascale Facility.

Supporting Information Available: Details of the Hybrid Monte Carlo method utilizing a polarizable potential and an alternate momentum resampling scheme. This material is available free of charge via the Internet at http://pubs.acs.org.

JA0737164

(87) Bhethanabotla, V.; Steele, W. *J. Phys. Chem.* **1988**, *92*, 3285.
(88) Widom, B. *J. Chem. Phys.* **1963**, *39*, 2808.
(89) Widom, B. *J. Phys. Chem.* **1982**, *86*, 869.